Shahrood University of Technology

Journal of Mining and Environment (JME)

Journal homepage: www.jme.shahroodut.ac.ir

Iranian Society of Mining Engineering (IRSME)

Bearing Capacity of Circular Footing Resting on Recycled Construction Waste Materials using ANN Method

Anant Saini[1], and Jitendra Singh Yadav[2*]

1. Department of Civil Engineering, National Institute of Technology Hamirpur, Himachal Pradesh, India
2. Department of Civil Engineering, National Institute of Technology Kurukshetra, Haryana, India

Article Info

Received 9 August 2023
Received in Revised form 22 October 2023
Accepted 7 November 2023
Published online 7 November 2023

DOI: 10.22044/jme.2023.13453.2485

Keywords

Construction waste materials
Circular footing
Bearing capacity
ANN
MLR

Abstract

The goal of this research work was to use an Artificial Neural Network (ANN) model to predict the ultimate bearing capacity of circular footing resting on recycled construction waste over loose sand. A series of plate load tests were conducted by varying the thickness of two sizes of recycled construction waste (5 mm and 10.6 mm) layer (0.4d, 0.6d, 0.8d, 1d, and 1.2d, d: diameter of footing) prepared at different relative densities (30%, 50%, and 70%) overlaying. The ultimate bearing capacity obtained for various combinations was used to develop the ANN model. The input parameters of the ANN model were thickness of recycled construction waste layer to diameter of circular footing ratio, angle of internal friction of sand, unit weight of sand, angle of internal friction of recycled construction waste and unit weight of recycled construction waste, and the model's output parameter was ultimate bearing capacity. The FANN-SIGMOD_SYMMETRIC model with topology 3-2-1 provided a higher estimate of the ultimate bearing capacity of circular footing, according to the ANN findings. The sensitivity analysis also revealed that the unit weight of sand and angle of internal friction of sand had insignificant effects on ultimate bearing capacity. The estimated ultimate bearing capacity was most affected by the angle of internal friction of recycled construction waste. The result of multiple linear regression analysis was not as good as the ANN model at predicting the ultimate bearing capacity.

1. Introduction

The foundation has always been the most crucial component of any construction, as it distributes the structural weight to the sub-surface soil layers. The weight should be dispersed such that neither the foundation nor the earth layers will collapse. Therefore, it is essential to evaluate the underlying soil's ability to support a load. It is crucial to understand how the foundation interacts with loose sand strata. The difficulty with building on loose sand is that, because of the pressure of the overburden, it may experience severe shear stress. Furthermore, the underlying structure probably has a high settlement value. As a result, before starting any project, settlement must be carefully assessed. Unsaturated, unconsolidated sediments that, when wet, quickly rearrange their particle sizes and drastically reduce in volume are referred to as loose or collapsible soil. Loose sand is susceptible to significant settlements because of its natural tendency to drain freely, which creates foundation problems. Therefore, a remedy must be used to increase the bearing capacity and reduce the related settlements [1].

Many different ground renovation methods are being employed to reinforce unstable soil layers and make them acceptable for building. Vibrolotation [2], grouting [3], cell confinement [4], geosynthetic material reinforcement [5], fibre reinforcement [6] [7], chemical stabilisation [8] [9] [10], and mechanical stabilization [11] [12] are a few of these methods. Blayi *et al.* [11] improved the strength of expansive soil by utilizing waste

Corresponding author: jsyadav@nitkkr.ac.in (J, Singh Yadav)

glass powder. Daraei *et al*. [13] stabilized the problematic soil by four cementitious materials including cement, quicklime, gypsum, and NaCl, and reported reduction in collapsibility. Further, Daraei *et al*. [14] stabilized the soil of swelling soil using the cement grout.

Some of these techniques are too expensive and complicated for a big project. Therefore, it is essential that sustainable and economical solutions be found. Utilising recycled construction waste (RCW) is one of the suggested solutions for the problem.

Crushed concrete, fractured and crushed masonry, and mixed demolition debris make up construction and demolition waste [15]. Construction and demolition waste were left behind after a structure has been built, restored or demolished. Additionally, municipal corporations all over the globe, particularly in India, where 53.13 million tonnes of municipal solid waste were created in 2017, are becoming increasingly concerned about how to handle and manage constructing and demolition waste due to its environmental impact. 31% of the total waste generated is inert waste, which includes demolition and construction debris. India produces 150 MT of demolition waste per year or 35–40% of the world's construction and demolish (C&D) waste [16]. Only around 1% of the construction and demolition debris generated in India gets recycled, according to the Centre for Science and Environment (CSE). Landfills are used to dispose of the remaining waste. Finding fresh approaches to re-establish ecological balance and safeguard the environment is thus crucial. In civil engineering applications, it may be obtained by recycling and reusing construction and demolition waste [17].

The usage of RCW fragment made from pulverised concrete is advised in building projects with several standards [18]. Construction and demolition waste's ability to reduce the need for raw material extraction is one of its most notable benefits. As a result, emissions of greenhouse gases and other pollutants have drastically lowered. Additionally, waste disposal facilities and related costs may be minimised. The replacement of unstable soil up to a large depth, low-lying land infill, sub-base for road building, etc. are only a few geotechnical uses for construction and demolition debris.

Geotechnical uses for C&D waste include fill material for retention structures, bank protection, subbase course material for paving, and more [15]. Arulrajah *et al*. [19] evaluated the geotechnical and geoenvironmental parameters of the C&D waste material employed as a pavement subbase. It was said that recycled concrete aggregate (RCA) was a more geotechnically sound material than conventional granular material and that it was also ecologically benign. The geotechnical properties of clayey soil were enhanced in a study by Jain and Chawda [20] by adding well-graded pulverised concrete aggregate (0.5%, 10%, and 25%), and the results were promising. Henzinger and Heyer [21] conducted an experiment to find out what happens when recycled demolition material is added to fine-grained soils. Low, medium, and high plasticity clay soils were combined with 50% recycled aggregate. With the addition, dry density and bearing capacity were observed. The findings showed that recycled aggregate functioned better in less plastic soils. The unconfined compressive strength and California bearing ratio of clay were found to be greatly improved by the addition of recycled concrete aggregate, dragged asphalt fragments, and natural gravel aggregate by Cabalar *et al*. [22]. Iqbal *et al*. [1] studied the geotechnical use of drinking water sludge (DWS) combined with crushed concrete (CC) and incinerator ash (IA). Among the experiments conducted in the lab were the California bearing ratio (CBR), undrained triaxial compression, compaction, and consolidation. In addition, an empirical equation for the maximum dry density and blending proportion was created. The consolidated undrained triaxial compression test results show that the addition of CC/IA to DWS increases friction angles but has no effect on the undrained shear strength. The compressibility of DWS is greatly reduced by the CC mix, especially in samples with more than 50% CC and CC/IA, according to consolidation experiments. CC and DWS are often utilised effectively as a road subgrade.

Recycled crushed concrete (CC), according to Karkush and Yassin [23], improved the geotechnical and chemical properties of porous soil. The porous soil samples underwent CC treatments of 5%, 10%, and 15%. The unconfined compressive strength (UCS) measurement was utilised to determine the shear strength characteristics of porous soil. 10% CC increased the chemical properties of soft soil, but bigger concentrations of CC significantly decreased those values even if they were still better than those of soft soil. The compaction curve may measure a maximum dry density of 1.81 g/cm^3 or 15% pulverised concrete. Pulverised concrete improved soil cohesion by reducing soil expansion and compression when mixed with loose soil. The

porous soil's shear strength and related compressibility increased by 175–193.5% and 25–31%, respectively. There hasn't been much study on the use of C&D residue in stabilising porous soil. By placing a CCD sand (CCD-S) composite on random sand, Sharma *et al*. [24] investigated the possibility of employing crushed concrete debris (CCD) as a foundation material. A direct shear test and a modified proctor test were each conducted in order to assess the shear strength parameters and the ideal CCD-S composite %. Additionally, plate load studies were conducted when a non-woven geotextile was used at the CCD-S mixture's interface. The experimental findings showed that the bearing capacity of sand was improved by 3.2 and 3.26 times, respectively, with the use of CCD-S composite and the insertion of geotextile at the interface. Sharma and Sharma [25] found that adding an appropriate amount of construction and demolition waste increased clayey soil's permeability and strength.

Old concrete that had been crushed and added, lowered the settlement and improved stiffness modulus more than bricks. Aljuari *et al*. [26] performed a numerical investigation on expanding soil by partially replacing it with concrete material using the Geo-Studio 2007 software. The depth of the crushed concrete layer, which varied from 20 to 70 cm with a 10-cm increment, and the amount of time needed for full expansion were among the several characteristics that were examined. Both evaluations of these parameters - with and without a footing - were performed. According to the research work, the thickness and width of the layers of pulverised concrete increased while the vertical swelling decreased. It was shown that applying pulverised concrete strata more successfully prevented the vertical expansion of high suction soil than low suction soil. Eventually, the vertical expansion decreased as the CC layers' thickness climbed. Three types of C&D wastes (dragged asphalt, crushed brick, and crushed concrete) were tested for their influence on the behaviour of a low-plasticity clay intended for use as a road subgrade layer by Al-Obaydi *et al*. [27] using a field California bearing ratio test. Crushed concrete was shown to be an effective addition and to increase CBR values more so than other debris.

A study by Shourijeh *et al*. [28] found that incorporating RCA into reinforced clay greatly increased its unconfined compressive and tensile strength. It was suggested that a mixture of 28-day-cured clay reinforced with 0.5% fibres and stabilised with 10% recycled concrete aggregates be used for subbase layers in both flexible and stiff pavements. Zhang *et al*. [29] evaluated the efficiency of C&D waste as aggregates in sulfate-alkali-activated polypropylene-fiber-reinforced cement-stabilized soil (CSS). The ideal percentages of Portland cement, polypropylene fibre, construction and demolition debris, and sodium sulphate were found to be 30%, 4%, 20%, and 0.8%, respectively. Soni *et al*. [30] evaluated the behaviour of square footing over recycled concrete aggregate resting on loose sand, and noticed that at a lower relative density, larger size aggregate performs better, and at higher relative density, smaller size aggregate performs better. Previous research has mostly focused on RCW's potential as a filler, a substitute for NCA in concrete, and a subgrade soil. The RCW has not been the subject of much study. The influence of RCW size variation has also not been well-investigated. Therefore, extensive numerical and experimental analysis is required to demonstrate the viability of using RCW as a foundation material.

Now adays, the use of artificial neural network is getting popularity in the civil engineering as well. Verma and Kumar [31] predicted the equation for the modified Proctor compaction parameters of fine-grained soil, and found that the propsed ANN model was more superior to those other models mentioned in the literature. Das and Basudhar [32] developed an artificial neural network model to predict the lateral load capacity of piles in clay. Three criteria were selected to compare the ANN model with the available empirical models: the best fit line for predicted lateral load capacity (Qp) and measured lateral load capacity (Qm), the mean and standard deviation of the ratio Qp/Qm, and the cumulative probability for Qp/Qm. Ornek *et al*. [33] used ANN technique for prediction of bearing capacity of circular footings on soft clay stabilized with granular soil. Similarly, for the prediction of ultimate bearing capacity of circular foundation on sand layer of limited thickness, Sethy *et al*. [34] used artificial neural network.

Further, Golewski [35] noticed the improvement in the strength parameters and microstructural properties of concrete with the inclusion of coal fly ash and Nanosilica. Further, the combined fly ash, silica fume, and Nano silica with ordinary Portland cement on the mechanical properties and brittleness of concrete were also studied by Golewski [36] [37] [38]. Golewski [39] described the main requirements for the construction of pocket foundation with particular

attention to the type of surface present inside the pocket. Wang *et al*. [40] represented fabrication and properties of concrete containing industrial waste. Haeri *et al*. [41] simulated the bluntness of TBM disc cutters in rocks using displacement discontinuity method. In another work, Haeri *et al*. [42] adopted a multilaminate based model to predict the the elasto-plastic behaviour of rock. Sarfarazi *et al*. [43] evaluated the tensile strength of concrete using a novel apparatus called as see - saw. Fu *et al*. [44] concluded that compressive strength of the of concrete is highly affected by the fracture pattern and failure mechanism assuming different configurations of the cracks and the hole locations. Sarfarazi [45] studied the effect of bedding layer on the tensile failure behaviour in hollow disc models using particle flow code.

In the last two decades, the use of recycled concrete waste (RCW) in applications such soil subgrade, filler material, and as a replacement for naturally occurring coarse aggregates (NCA) in concrete have been the subject of several research works. Regarding the use of RCW as a foundation material, research is noticeably lacking. Furthermore, the effects of various RCW particle sizes have not yet been fully investigated. The present study aims to predict the ultimate bearing capacity of circular footing resting over an RCW layer overlaying loose sand. The data obtained through plate load test was used to develop Artificial Neural Network (ANN) and multiple linear regression (MLR) models. In the plate load test, the effects of different parameters on the bearing capacity were evaluated including relative density (I_D = 30%, 50%, and 70%), thickness of RCW layer to diameter of circular footing ratio (u/d = 0.4, 0.6, 0.8, 1.0, 1.2; d: diameter of footing), and size of recycled construction waste (RCW) (5 mm and 10.6 mm) on the bearing capacity were assessed.

2. Research Methodology

2.1 Soft computing techniques

In this investigation, the ultimate bearing capacity of circular footing resting on recycled construction waste over loose sand was predicted by utilising the two soft computing methodologies. The primary purpose of ANN modelling is to predict an undetermined outcome based on the input data. To predict the outcome, software requires a set of variables and the results of scientific research. An ANN requires at least three layers to function correctly. Information-receiving neurons are located in the upper layer. To evaluate the accuracy of the network's current operation, two sets of data are required. To determine the number of concealed layers and neurons, however, only a handful of methods were reported in the scientific literature. In this investigation, Boger and Guttman's [46] rule of thumb was applied. According to Boger and Guterman [46], 70% (or 2/3rds) of the extent of the input layer can be assumed to be the number of neurons in the hidden layers. The output of a neuron is dependent from the activation function chosen. Metrics including root mean square error (RMSE), mean absolute percentage error (MAPE), mean absolute error (MAE), and mean square error (MSE) are used to quantify performance, with lower values suggesting higher activation function efficacy. Accuracy levels are determined by MAPE values. The MAPE values of less than 10%, between 10% and 20%, between 20% and 50%, and greater than 50% were considered accurate, good, acceptable, and imprecise, respectively [47]. The evaluation of ANN models makes use of correlation coefficient (r) and the coefficient of determination (R^2). The error models used to anticipate the ultimate bearing capacity using a neural network approach are displayed in Table 1. The Agiel neural network software was used in this study.

Multiple linear regression analysis (MLRA) is used to determine the optimal relationship between a single continuous dependent variable and two or more continuous dependent variables. This study examined the relationship between the ultimate bearing capacity of circular footing (dependent variable) and u/d ratio, angle of internal friction and unit weight of RCW and sand (independent variables) using SPSS 12.0.

Given n observations, the following is a general model for calculating the MLRA.

$$\mu_y = \beta_o + \beta_1 x_1 + \beta_2 x_2 + \beta_3 x_3 \ldots + \beta_n x_n \quad \text{(i)}$$

where μ_y represents the dependent variable, x_i represents the independent variables, and β_i represents the predicted parameters, respectively.

2.2. Data collection

A set of plate load tests were carried out in laboratory to determine the ultimate bearing capacity of circular footing resting over an RCW layer overlaying loose sand. The physical properties of the sand, and RCW (5 mm and 10.6 mm) obtained from laboratorial tests performed in cord with various Indian Standards is tabulated in Table 2. Figure 1(a) and (b) show the RCW used in this study. The friction angle of RCW-II was

smaller than RCW-I at RD = 50% and 70%. The higher values of friction angle of RCW-I compared to RCW-II may be perhaps attributed to better interaction among the particles of RCW-I due to the large specific surface area. However, further investigation is required to be conducted for the in-depth study. The observed behaviour of RCW under shear was contrary to the results reported by Islam *et al*. [48]. The authors observed decrease in the angle of internal friction of cohesionless soil with the increase of effective size at lower densities. Further, at higher density of cohesion less soil, an increment in the angle of internal friction was seen with the increase of effective particle size.

Table 1 Various statistical parameters and error models

Statistical parameter	Mathematical expression
Correlation coefficient (r)	$r = \frac{\sum Q_{ut_i}.Q_{up_i} - n\overline{Q_{ut}}.\overline{Q_{up}}}{(n-1)S_{Q_{ut}}.S_{Q_{up}}}$
Coefficient of determination (R^2)	$R^2 = 1 - \frac{\sum_i \left(Q_{up_i} - Q_{ut_i}\right)^2}{\sum_i \left(Q_{up_i} - \overline{Q_{up}}\right)^2}$
Mean square error (MSE)	$MSE = \frac{1}{n}\sum_{i=1}^{n} \left(Q_{ut_i} - Q_{up_i}\right)^2$
Root mean square error (RMSE)	$RMSE = \sqrt{\frac{1}{n}\sum_{i=1}^{n} (Q_{ut_i} - Q_{up_i})}$
Mean absolute error (MAE)	$MAE = \frac{1}{n}\sum_{i=1}^{n} \left\|Q_{ut_i} - Q_{up_i}\right\|$
Mean absolute percentage error (MAPE)	$MAPE = \left[\frac{1}{n}\sum_{i=1}^{n} \left\|\frac{Q_{ut_i} - Q_{up_i}}{Q_{ut_i}}\right\|\right] \times 100$

Note: Q_{ut} Q_{up}: target and predicted Q_u respectively, $\overline{Qut}$, $\overline{Qup}$: mean of the target and predicted Q_u respectively, S_{Qut}, S_{Qup}: standard deviation of the target and predicted Q_u and n: is the number of observations

Table 2 Physical properties of the sand, RCW-I and RCW-II

Properties		Value		
		Sand	**RCW-I**	**RCW-II**
Specific gravity, Gs		2.60	2.65	2.70
Grain-size distribution				
Clay (< 2 µm)		-	-	-
Silt (2-75 µm)		2.7	-	-
Sand (0.075- 4.75 mm)		97.3	-	-
Gravel (> 4.75 mm)		-	100	100
Coefficient of curvature, Cc		1.01	0.96	0.93
Coefficient of uniformity, Cu		1.73	1.55	1.49
Classification		SP	GP	GP
	Relative density (%)			
Angle of internal friction	30	32.1°	38.3°	40.4°
	50	-	44.8°	41.7°
	70	-	50.2°	49.1°
	Relative density (%)			
Unit weight (kN/m^3)	30	13.60	11.63	12.67
	50	-	12.15	13.20
	70	-	12.66	13.75

Figure 1 (a) RCW -5 mm; (b) RCW-10.6 mm; (c) Prepared sand test bed, (d) Prepared RCW test bed; (e) Test setup

The model circular footing of cast iron of 80 mm diameter and 10 mm thickness was used. The plate load test was carried out in a testing tank with interior dimensions of 700 mm x 450 mm x 600 mm (as shown in Figure 1(e)). The testing tank was filled with two different layers. The loose sand and

RCW were poured at the lower and upper layers of the tank, respectively. To maintain the loose behaviour of the sand, the tank was filled with sand in three equal layers using the raining technique up to the required height [49] [24] [50]. The upper side encompasses RCW was placed over the prepared sand bed (Figure 1(d)). Prior to the experiment, the appropriate relative density was established by a series of tests with various fall heights. In each trial, densities were measured by taking samples in known-volume aluminium cups that were positioned at various points in the test tank. Based on the marked height in the tank and the initial density (30%), the weight of the sand was determined. The sand was meticulously levelled once it had been filled to the desired height of 450 mm. Standard-sized containers were set up at various locations throughout the tank to measure the sand's unit weight. After that, the prepared sand bed was covered with a layer of RCW. Utilising the unit weight and the volume of the RCW, the weight corresponding to a certain relative density for each RCDW layer was calculated. A 6 N wooden rammer was used to manually compress the RCDW after it had been manually poured to fill the layer from a constant height [50] [30]. The test was carried out on the prepared sand bed using a load cell and strain-controlled loading frame of capacity 5 kN and 50 kN, respectively. All tests were conducted using a strain rate of 0.24 mm/min. The test was carried out up to a settlement of 20% of the footing diameter. For more details regarding the testing assembly and preparation of testing tank have already been published [30]. The influence of various parameters such as relative density (ID = 30%, 50%, and 70%), thickness of RCW layer to diameter of circular footing ratio (u/d = 0.4, 0.6, 0.8, 1.0, 1.2; D: diameter of footing), and size of RCW (5 mm and 10.6 mm) on the bearing capacity were assessed. The obtained pressure-settlement behaviour of circular footing resting on loose sand overlaying RCW of 5 mm and 10.6 mm at u/d = 1.2 is shown in Figure 2(a) and 2(b), respectively. To develop the ANN model of the study, the input parameters were taken as u/d, ϕ_1 (angle of internal friction of sand), γ_1 (unit weight of sand), ϕ_2 (angle of internal friction of RCW), and γ_2 (unit weight of RCW), and output parameter was ultimate bearing capacity. The dataset used for this investigation is shown in Table 3.

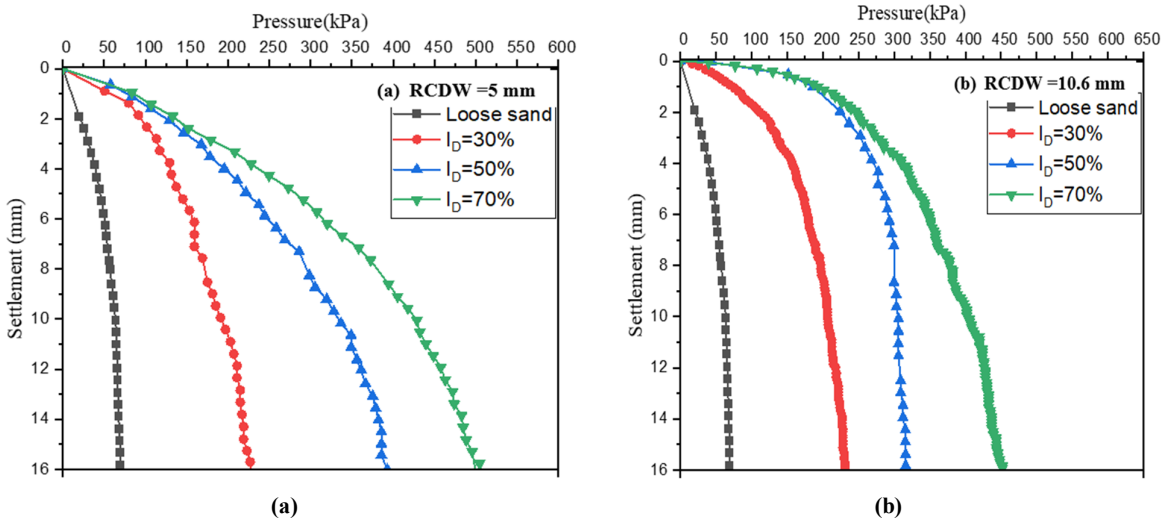

(a) (b)

Figure 2 Pressure-settlement behaviour of circular footing resting on loose sand overlaying RCW at u/d =1.2 (a) 5 mm (b) 10.6 mm

Table 3 Data set used for modelling

Input parameters					Output parameter
u/d	ϕ_1 (°)	γ_1 (kN/m^3)	ϕ_2 (°)	γ_2 (kN/m^3)	q_{ult} (kN/m^2)
0	32.1	13.86	0	0	62.18
0.4	32.1	13.86	38.3	11.86	99.8
0.6	32.1	13.86	38.3	11.86	121
0.8	32.1	13.86	38.3	11.86	156
1	32.1	13.86	38.3	11.86	174
1.2	32.1	13.86	38.3	11.86	198
0.4	32.1	13.86	44.8	12.39	138
0.6	32.1	13.86	44.8	12.39	212
0.8	32.1	13.86	44.8	12.39	241
1	32.1	13.86	44.8	12.39	285
1.2	32.1	13.86	44.8	12.39	319
0.4	32.1	13.86	50.2	12.91	207.1
0.6	32.1	13.86	50.2	12.91	286.2
0.8	32.1	13.86	50.2	12.91	339.21
1	32.1	13.86	50.2	12.91	359
1.2	32.1	13.86	50.2	12.91	398
0.4	32.1	13.86	40.4	12.92	108
0.6	32.1	13.86	40.4	12.92	138.3
0.8	32.1	13.86	40.4	12.92	161.2
1	32.1	13.86	40.4	12.92	197
1.2	32.1	13.86	40.4	12.92	206.5
0.4	32.1	13.86	41.7	13.46	118
0.6	32.1	13.86	41.7	13.46	181
0.8	32.1	13.86	41.7	13.46	210
1	32.1	13.86	41.7	13.46	244
1.2	32.1	13.86	41.7	13.46	285
0.4	32.1	13.86	49.1	14.02	195.8
0.6	32.1	13.86	49.1	14.02	251.9
0.8	32.1	13.86	49.1	14.02	291.8
1	32.1	13.86	49.1	14.02	329.5
1.2	32.1	13.86	49.1	14.02	365.8

3. Result and Discussion

3.1. Ultimate bearing capacity equation using artificial neural network

Based on the results obtained through model plate load test, the Agiel neural network software [51] was employed to predict the ultimate bearing capacity of circular footing resting on RCW over loose sand. For training and testing purposes, 70% and 30% data obtained through numerical analysis were taken.

In this investigation, Boger and Guterman's [46] rule of thumb was utilised. The number of hidden layers and the number of neurons in each hidden layer were determined to be 1 and 4, respectively, based on the Boger and Guterman's [46] research work. Next, the number of epochs for the neural network model must be determined. To avoid training-induced noise and poor prediction, it became crucial to determine when to stop training. A trial-and-error approach was used to determine the required number of data training and evaluation iterations. The mean square error (MSE) between ANN predictions and target values was calculated using distinct epoch values. Only the training data with the lowest MSE value would be used to determine the structure of the neural network model. When the values of epochs decreased, training was discontinued. Given the aforementioned information, 950 epochs and a 5-4-1 topology ANN model were chosen for training. Figure 3 depicts the proposed neural network model's topology. This study investigates the

performance of artificial neural network structures with varying activation functions. The ultimate bearing capacity was determined by trial and error for both training and testing sets at 950 repetitions. It takes longer to accomplish the iteration procedure the more trials are conducted. In this investigation, the algorithm's default learning rate was set to 0.7. As shown in Tables 4 and 5, the efficacy of various activation functions was predicted for training and assessment datasets.

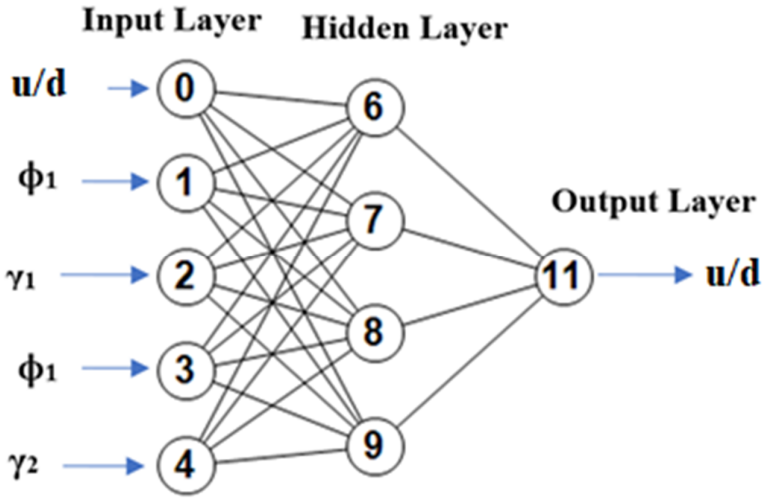

Figure 3 5-4-1 Topology of the artificial neural network model

Table 4 Performance measures for various activation function for the training data

Activation Function	r	r^2	MSE	RMSE	MAE	MAPE (%)
FANN-Linear	0.78	0.19	4322.08	65.74	53.13	24.08
FANN-THRESHOD	-1.90E-16	-6E+32	30637.87	175.04	155.78	254.42
FANN-THRESHOD-SYMMETRIC	2.73E-16	-2E+32	218294.7	467.22	460.35	189.18
FANN-SIGMOID	0.97	0.96	212.62	14.58	11.06	6.08
FANN-SIGMOD_STEPWISE	0.97	0.97	195	13.96	11.41	6.22
FANN-SIGMOD_SYMMETRIC	0.97	0.96	222.97	14.93	10.28	5.16
FANN-SIGMOD_ SYMMETRIC_STEPWISE	0.96	0.93	397.99	19.95	14.23	7.23
FANN-GAUSSIAN	0.99	0.97	201.67	14.2	10.93	5.81
FANN_GAUSSIAN_SYMMETRIC	0.99	0.96	269.24	16.41	11.44	6.57
FANN-GAUSSIAN_STEPWISE	-1.90E-16	-6E+32	30637.87	175.04	155.78	254.42
FANN_ELLIOT	0.91	0.91	436.12	20.88	16.39	9.64
FANN_ELLIOT_SYMMETRIC	0.89	0.85	693.07	26.33	18.81	9.56
FANN_LINEAR_PIECE	0.32	-14.92	15404	124.11	110.75	35.33
FANN-LINEAR_ PIECE_SYMMMETRIC	0.81	0.35	3508.18	59.23	46.85	21.07
FANN_SIN_SYMMETRIC	0.97	0.87	860.18	29.33	22.15	12.04
FANN_COS_SYMMETRIC	0.98	0.95	288.28	16.98	13.14	8.19
FANN_SIN	1	0.95	307.23	17.53	12.91	7.03
FANN_COS	0.53	-0.61	4520.35	67.23	44.4	17.87

Table 5 Performance measures for various activation function for the testing data

Activation Function	r	r^2	MSE	RMSE	MAE	MAPE (%)
FANN-Linear	0.98	0.96	259.85	16.12	12.23	6.61
FANN-THRESHOD	-1.90E-16	-2.71	7310.22	85.5	69.86	26
FANN-THRESHOD-SYMMETRIC	2.73E-16	-3.05	11101.07	105.36	85.73	28.33
FANN-SIGMOID	0.97	0.96	205.75	14.34	11.27	6.27
FANN-SIGMOD_STEPWISE	1	0.99	73.57	8.58	6.34	3.21
FANN-SIGMOD_SYMMETRIC	1	0.99	51.7	7.19	5.74	2.49
FANN-SIGMOD_ SYMMETRIC_STEPWISE	0.97	0.96	211.48	14.54	10.65	5.28
FANN-GAUSSIAN	0.99	0.96	239.81	15.49	10.5	5.45
FANN_GAUSSIAN_SYMMETRIC	0.98	0.96	216.93	14.73	10.43	5.7
FANN-GAUSSIAN_STEPWISE	-1.90E-16	-2.3E+30	7418.6	86.13	70.65	28.33
FANN_ELLIOT	0.97	0.97	190.72	13.81	11.02	5.96
FANN_ELLIOT_SYMMETRIC	0.97	0.96	205.96	14.35	11.28	6.22
FANN_LINEAR_PIECE	0.82	0.49	3226.88	56.81	46.9	18.92
FANN-LINEAR_ PIECE_SYMMMETRIC	0.98	0.95	322.65	17.96	13.45	7.17
FANN_SIN_SYMMETRIC	0.98	0.95	330.29	18.17	14.76	8.81
FANN_COS_SYMMETRIC	0.98	0.95	298.16	17.27	14.46	8.56
FANN_SIN	0.98	0.95	332.28	18.23	14.68	8.8
FANN_COS	0.6	-0.23	4177.39	64.63	44.75	17.74

The efficacy of each activation function was predicted based on Tables 4 and 5 for both the training and testing data sets. The FANN-SIGMOD_SYMMETRIC function had the highest correlation coefficient (r), determination coefficient (R^2), and the lowest MAPE, RMSE, MAE, and MAPE values among all the activation functions in the current investigation. The statistical values for FANN-SIGMOD_SYMMETRIC training and testing data are displayed in Table 6. Figure 4 depicts the relationship between the predicted and desired ultimate bearing capacity in the training and testing data set for the FANN-SIGMOD_SYMMETRIC activation function with 5-4-1 topology.

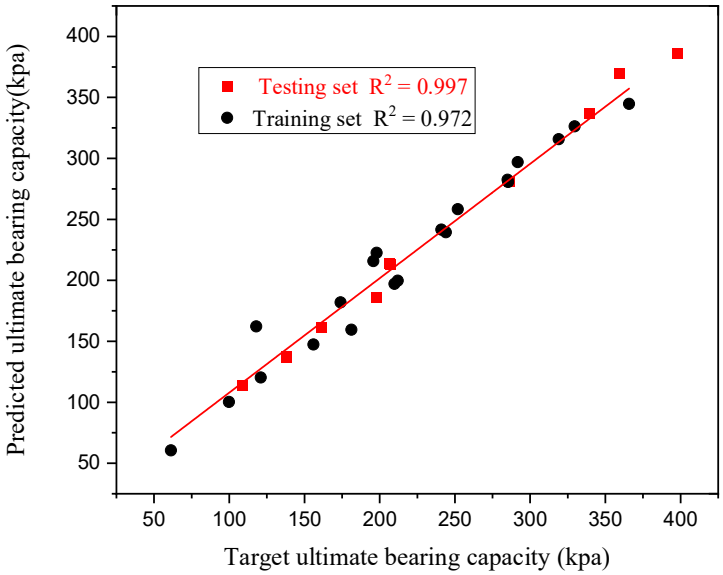

Figure 4 Prediction and target ultimate bearing capacity circular footing resting in sand overlying RCDW in the training and testing data set using ANN

Table 6 Statistical values for the training and testing data for the best activation function

Statistical Values	FANN-SIGMOD SYMMETRIC Function	
	Training data	Testing data
r	0.97	0.99
R^2	0.96	0.99
MSE	222.97	51.70
RMSE	14.93	7.19
MAE	10.27	5.73
MAPE	5.16%	2.48%

Using a technique described by Garson [52], a sensitivity analysis was conducted to determine the influence of individual parameters on compression capacity. This method's output was determined by absolute weight. To circumvent this issue, Olden and Jackson [53] proposed a new method termed "Relative Importance," which computes the total of the final weights between hidden layer neurons and output neurons based on the weight of the connection between the input parameter and hidden layer neurons. The calculation is as follows:

$$RI_j = \sum_{k=1}^{h} w_{jk} \times w_k \qquad \text{(ii)}$$

where:

RI_j = Relative importance of j^{th} input layer neuron

w_k = Weight of connection between k^{th} hidden layer neuron and output neuron

w_{jk} = Weight of connection between j^{th} input parameter and k^{th} hidden layer neuron

h = Number of neurons in hidden layer

b_{hk} = Bias at the kth hidden layer neuron

On the basis of the neural network model's weights, the impact of five input variable quantities on the predicted capacity was investigated. Table 7 displays the weight of connection between the input parameter and hidden layer neuron, as well as between the hidden layer neuron and output neuron, for the FANN-SIGMOD_SYMMETRIC function. Figure 5 depicts the relative relevance of each parameter of the FANN-SIGMOD_SYMMETRIC function based on the ANN model of output ultimate bearing capacity. The analysis of Figure 5 reveals that the ϕ_2 is the most significant parameter, followed by γ_2 and u/d. Further, it can be concluded that ϕ_1 and γ_1 are indirectly proportional to the predicted ultimate bearing capacity.

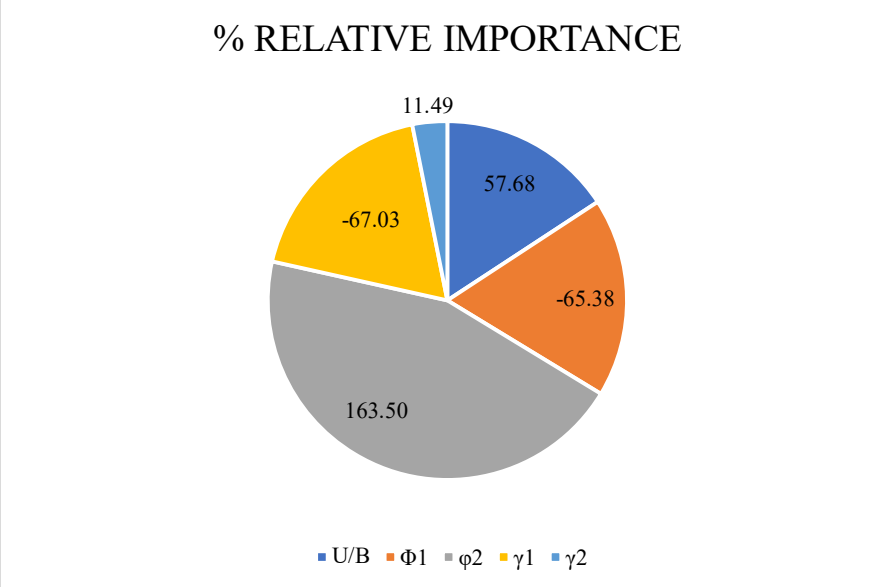

Figure 5 Individual variables' relative importance in determining ultimate bearing capacity

Table 7 Final weights between the input neuron and hidden neuron as well as hidden neuron and output neuron

Neuron	Weights (w_{jk})						Biases	
	q_u	u/d	ϕ_1	γ_1	ϕ_2	γ_2	B_{hk}	B_o
Hidden 1	-1.6249	-0.9873	0.3224	0.3217	-1.7300	-0.3135	0.292864	0.118797
Hidden 2	-2.9684	-1.1400	1.2321	1.1816	-3.9935	-0.4271	1.10773	-
Hidden 3	-2.3537	-1.5060	0.7649	0.6486	-2.4040	-0.3581	0.74467	-
Hidden 4	7.2176	2.3686	-3.2147	-3.3720	7.2871	0.3475	-3.24335	-

The primary equation of the ANN model relating the input parameter to the output ultimate bearing capacity is:

$$q_{ult} = f\{b_0 + \sum_{k=1}^{h}(w_k * f[b_{hk} + \sum_{f=1}^{m}(w_{jk} * X_j)])\} \quad \text{(iii)}$$

q_{ult} = Ultimate bearing capacity

f = Activation function

bo = Weight of output layer bias

bhk = Weight of kth hidden layer neuron

m = Number of neurons in the output layer

Xj = standardized input parameter j in ranges between (-1 and 1).

The model equation for the ultimate bearing capacity of a circular footing resting on RCW laying sand was derived using the weights and biases listed in Table 7, and the following expressions were drawn:

$$A = 0.292864 - 0.98738 * u/d + 0.322417 * \phi_1 - 1.73009 * \phi_2 + 0.321734 * \gamma_1 - 0.31353 * \gamma_2$$

$$B = 1.10773 - 1.14006 * u/d + 1.232151 * \phi_1 - 3.99357 * \phi_2 + 1.181644 * \gamma_1 - 0.42718 * \gamma_2$$

$$C = 0.74467 - 1.50605 * u/d + 0.764958 * \phi_1 - 2.40405 * \phi_2 + 0.648686 * \gamma_1 - 0.35817 * \gamma_2$$

$$D = -3.24335 + 2.368647 * u/d - 3.214743614 * \phi_1 + 7.287144 * \phi_2 + 23.37206 * \gamma_1 + 0.347514 \gamma_2$$

$$E = 0.118797 - 1.624965\{2/(1 + \exp(-2 * 0.5 * A)) - 1\} - 2.968484\{2/(1+\exp(-2 * 0.5 * B)) - 1\} - 2.353736\{2/(1+\exp(-2 * 0.5 * C)) - 1\} + 7.217616\{2/(1 + \exp(-2 * 0.5 * D)) - 1\}$$

$$q_{ult} = 2/(1+\exp(-2 * 0.5 * E)) - 1 \quad \text{(iv)}$$

The value q_{ult} determined by Equation (iv) was between 0 and 1 for the FANN-SIGMOD_SYMMETRIC activation function. To obtain the actual ultimate bearing capacity, the following denormalization of Equation (iv) was performed:

$$Q(kPa) = 0.5(q_{ult} + 1)\,(q_{ultmax} - q_{ultmin}) + (q_{ultmin}) \quad \text{(v)}$$

where q_{ultmax} and q_{ultmin} are the maximum and minimum ultimate bearing capacity, respectively.

According to the results of the sensitivity analysis, ϕ_1 and γ_1 have a negative impact on the predicted ultimate bearing capacity, resulting in a low degree of simplification. The neural network was modified by ignoring the ϕ_1 and γ_1. This approach is consistent with Dutta *et al*. [54]. The revised neural network input parameters were ϕ_2, γ_2, and u/d, and the ANN model output parameter was the ultimate bearing capacity. Two variables were eliminated from the revised network. Consequently, the number of neurons in the hidden layer was revised to two. The topology of the revised neural network structure was 3-2-1. The training and evaluating dataset used for the revised 3-2-1 topology model must be identical to that of the prior model.

The previous model's parameters including the number of Epochs, learning rate, and activation function were retained. The efficacy of the FANN-SIGMOD_SYMMETRIC activation function was predicted for revised models' training and testing datasets. Table 8 presents the statistical values of training and testing data for the revised topology. Table 9 displays the final weight of connection between the input parameter and hidden layer neuron and the hidden layer neuron and output neuron of the revised neural network. Figure 6 depicts the graphical relationship between the predicted and target ultimate bearing capacity of circular footing for the training and testing datasets of the revised neural network with 3-2-1 topology.

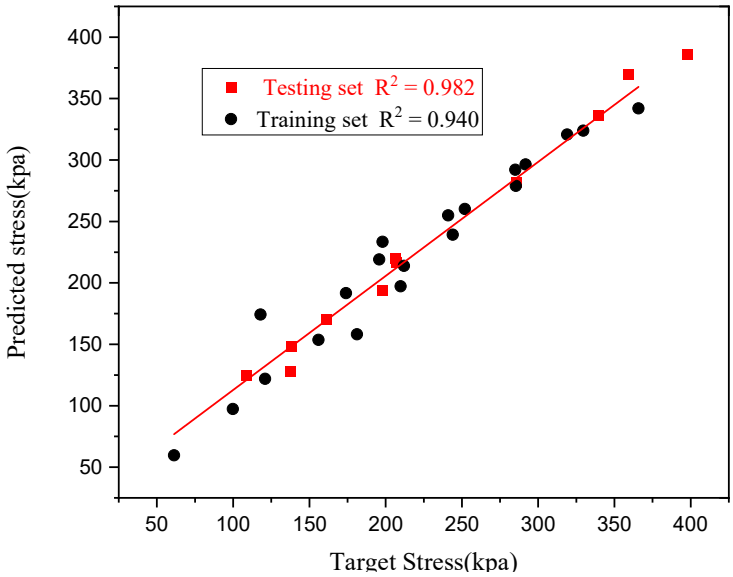

Figure 6 Predicted and target ultimate bearing capacity of circular footing resting in sand overlying RCDW in the training and testing data set using FANN-SIGMOD_SYMMETRIC activation function with 3-2-1 topology

Table 8 Revised Statistical values for the training and testing data for the best activation function

Statistical Values	FANN-SIGMOD_SYMMETRIC Function	
	Training data	Testing data
r	0.97	0.99
R^2	0.93	0.98
MSE	348.53	102.79
RMSE	18.66	10.13
MAE	12.67	9.38
MAPE	6.13	4.93

3.2. Proposed model equation for ultimate bearing capacity based on revised neural network model:

Using the values of the weights and biases shown in Table 9, the revised model equation for the ultimate bearing capacity of circular footings resting on RCW overlying loose sand was derived using the following expressions:

$$A = 7.14334 + 1.989437 * u/d + 5.973646164 * \phi_2 + 0.9220095 * \gamma_2$$

$$B = 0.374737 - 0.58188 * u/d + 0.044099387 * \phi_2 + 1.3622297 * \gamma_2$$

$$C = 3.64839 + 3.735568\{2/(1+\exp(-2 * 0.5 * A)) - 1\} + 0.3828716\{2/ (1 + \exp(-2 * 0.5 * B)) - 1\}$$

$$q_{ult} = 2/(1+\exp(-2 * 0.5 * C)) - 1 \quad \text{(vii)}$$

$$Q(kPa) = 0.5(q_{ult} + 1) (q_{ultmax} - q_{ultmin}) + (q_{ultmin}) \quad \text{(vi)}$$

Table 9 Final weights between the input neuron and hidden neuron as well as hidden neuron and output neuron for revised neural network having topology 3-2-1

Neuron	Weights (w_{jk})				Biases	
	q_u	u/d	ϕ_2	γ_2	B_{hk}	B_o
Hidden 1	3.735568	1.989437	5.973644	-0.9220095	-7.14334	3.648398
Hidden 2	0.3828716	-0.58118	-0.0440987	-1.3622297	0.374737	

The limitations of the proposed ANN model are as follows:

- The proposed model is valid for RCW of 5 mm and 10.6 mm.
- u/d is limited up to 1.2.
- The underlaying sand is in loose state (i.e. I_D = 30%).
- The bearing capacity offered by the underlaying sand was neglected.
- Proposed model is valid for circular footing only.
- Effect of water table is not considered.

3.3 Ultimate bearing capacity equation using multiple linear regression

Using the SPSS software, multiple linear regression (MLR) was performed on training and testing data. The used data was identical to that of the artificial neural network model. The multiple regression analysis input parameters were ϕ_2, γ_2, and u/d, and the output parameter was ultimate bearing capacity.

Using multiple linear regression analysis, the input and output parameters of training data were examined. The resulting model equation was:

$$q_{ult} = 170.781(u/d) + 11.896\ \phi_2 - 0.355\ \gamma_2 + 17.587 \quad \text{(viii)}$$

The input variables of the training and testing datasets were entered into Equation (vii), and the output ultimate bearing capacity was computed. Figure 7 depicts the relationship between the predicted and target ultimate bearing capacity of circular footings resting on RCW and coarse sand for the training and testing data sets using multiple linear regression.

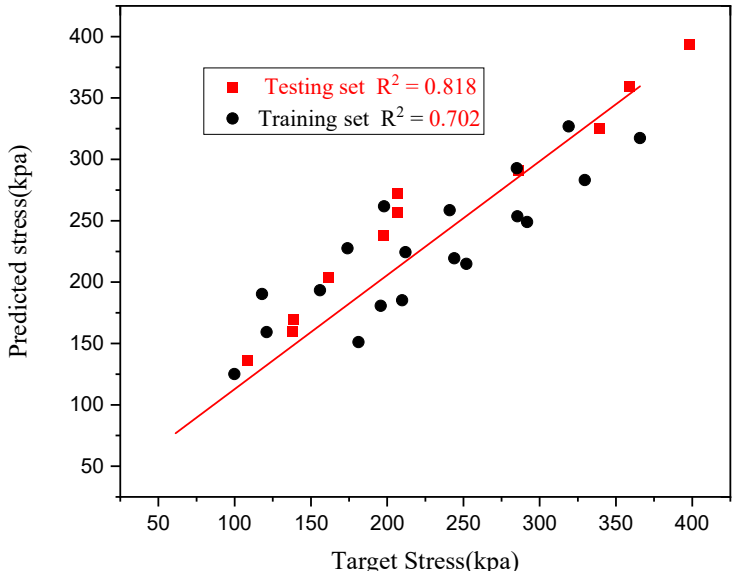

Figure 7 Predicted and target q_{ultp} of ultimate bearing capacity in the training and testing data set using multiple regression analysis

3.4. Comparison of regression using neural network model and multiple linear regression

Using the multiple linear regression method, the different performance measures were estimated based on data from training and testing. Performance measures were used to compare the updated neural network model and the multiple linear regression. Table 10 shows a comparison of the statistical values of the updated 3-2-1 topology neural network model and the multiple regression analysis.

Table 10 Comparison of statistical coefficients between revised neural network model having 3-2-1 topology and multiple regression analysis

Performance measures	Prediction model			
	Revised neural network (Topology 3-2-1)		Multiple regression analysis	
	Training data	Testing data	Training data	Testing data
r	0.97	0.99	0.88	0.98
R^2	0.94	0.98	0.7	0.82
MSE	348.54	102.8	1460.15	1162.06
RMSE	18.67	10.14	38.21	34.09
MAE	12.68	9.39	34.03	27.63
MAPE	6.13	4.94	27.32	12.85

Table 10 shows that the performance of an updated neural network with structure 3-2-1 is better than that of a network made with multiple linear regression. R^2 and MAPE obtained from revised neural network was better than obtained from multiple linear regression. R^2, for revised neural network, was 0.94 for training data and 0.98 for testing data, whereas for multiple linear regression, the values were 0.7 and 0.82, respectively. Similar, MAPE, for revised neural network was 6.13% for training data and 4.94% for testing data, whereas for multiple linear regression, the values were 27.32% and 12.85%, respectively. Thus, multiple regression analysis was not as good as the ANN model at predicting ultimate bearing capacity.

4. Conclusions

Based upon the above findings, the conclusions are as follows:

- With the increase in the relative density, thickness of RCW the bearing capacity of loose sand increases. The size of RCW also plays a vital role in the improvement of bearing capacity as well.
- The ultimate bearing capacity values predicted by the FANN-SIGMOD_SYMMETRIC activation function is closer to the actual ultimate bearing capacity.
- Analysis of sensitivity revealed that the angle of internal friction of sand and unit weight of ratio has a smaller effect on the predicted capacity.
- Angle of internal friction of RCW contributes the most to the predicted capacity.
- The revised neural network model with topology 3-2-1 provides superior output prediction than multiple regression analysis.

From the above-mentioned conclusion, it can be summarized that the bearing capacity of footing resting on RCW underlaying sand is mainly depend upon the angle of internal friction of RCW and thickness of RCW layer. In the present work, only two sizes of RCW were considered, i.e. 5 mm and 10.6 mm. The effect of brick waste and other type of RCW on the bearing capacity need to be investigated. The underlaying sand was assumed to in loose state (i.e. I_D = 30%). Future work addressing the effect of medium and dense sand on the bearing capacity need to be investigated. Insufficient amount of research work has been carried out on the combined effect of RCW mixed with sand to improve the bearing capacity of soil.

References

[1]. Abid, S. (2017). Stabilization of Soil Using Chemical Methods. *International Journal of Recent Trends in Engineering and Research*, *3*(9), 104–121.

[2]. Al-Obaydi, M. A., Abdulnafaa, M. D., Atasoy, O. A., & Cabalar, A. F. (2022). Improvement in Field CBR Values of Subgrade Soil Using Construction-Demolition Materials. *Transportation Infrastructure Geotechnology*, *9*(2), 185–205.

[3]. Aljuari, K. A., Fattah, M. Y., & Ali, H. E. (2021). Numerical Analysis of Treatment of Highly Expansive Soil by Partial Replacement with Crushed Concrete. *IOP Conference Series: Earth and Environmental Science*, *856*(1).

[4]. Angurana, D. I., Yadav, J. S., & Khatri, V. N. K. (2023). Estimation of Uplift Capacity of Helical Pile Resting in Cohesionless Soil. *Transportation Infrastructure Geotechnology*.

[5]. Arulrajah, A., Piratheepan, J., Disfani, M. M., & Bo, M. W. (2013). Geotechnical and Geoenvironmental Properties of Recycled Construction and Demolition Materials in Pavement Subbase Applications. *Journal of Materials in Civil Engineering*, *25*(8), 1077–1088.

[6]. Blayi, R. A., Sherwani, A. F. H., Ibrahim, H. H., Faraj, R. H., & Daraei, A. (2020). Strength improvement of expansive soil by utilizing waste glass powder. *Case Studies in Construction Materials*, *13*, e00427.

[7]. Boger, Z., & Guterman, H. (1997). Knowledge extraction from artificial neural networks models. *Proceedings of the IEEE International Conference on Systems, Man and Cybernetics*, *4*, 3030–3035.

[8]. Cabalar, A. F., Zardikawi, O. A. A., & Abdulnafaa, M. D. (2019). Utilisation of construction and demolition materials with clay for road pavement subgrade. *Road Materials and Pavement Design*, *20*(3), 702–714.

[9]. Cardoso, R., Silva, R. V., Brito, de J., & Dhir, R. (2016). Use of recycled aggregates from construction and demolition waste in geotechnical applications: A literature review. *Waste Management*, *49*, 131–145.

[10]. Chaudhary, V., Yadav, J. S., & Dutta, R. (2023). Geotechnical properties of bentonite mixed with nanosilica. *Multiscale and Multidisciplinary Modeling, Experiments and Design*, (2016).

[11]. Daraei, A., Herki, B. M. A., Sherwani, A. F. H., & Zare, S. (2018). Slope Stability in Swelling Soils Using Cement Grout: A Case Study. *International Journal of Geosynthetics and Ground Engineering*, *4*(1), 0.

[12]. Daraei, A., Sherwani, A. F. H., Faraj, R. H., Mohammad, S., Kurdo, S., Zare, S., & Mahmoodzadeh, A. (2019). Stabilization of problematic soil by utilizing cementitious materials. *Innovative Infrastructure Solutions*, *4*(1).

[13]. Das, S. K., & Basudhar, P. K. (2006). Undrained lateral load capacity of piles in clay using artificial neural network. *Computers and Geotechnics*, *33*(8), 454–459.

[14]. Dash, S. K., Rajagopal, K., & Krishnaswamy, N. R. (2004). Performance of different geosynthetic reinforcement materials in sand foundations. *Geosynthetics International*, *11*(1), 35–42.

[15]. Debats, J. M., & Sims, M. (1997). Vibroflotation in reclamations in Hong Kong. *Ground Improvement*, *1*(3), 127–145.

[16]. Dutta, R. K., Dutta, K., & Jeevanandham, S. (2015). Prediction of Deviator Stress of Sand Reinforced with Waste Plastic Strips Using Neural Network. *International Journal of Geosynthetics and Ground Engineering*, *1*(2). https://doi.org/10.1007/s40891-015-0013-7

[17]. Dutta, R. K., & Yadav, J. S. (2021). The impact of alccofine inclusion on the engineering properties of bentonite. *Cleaner Engineering and Technology*, *5*, 100301. https://doi.org/10.1016/j.clet.2021.100301

[18]. Fu, J., Haeri, H., Sarfarazi, V., Asgari, K., Ebneabbasi, P., Fatehi Marji, M., & Guo, M. (2022). Extended finite element method simulation and experimental test on failure behavior of defects under uniaxial compression. *Mechanics of Advanced Materials and Structures*, *29*(27), 6966–6981.

[19]. Ganiron, T. U. J. (2015). Recycling Concrete Debris from Construction and Demolition Waste. *International Journal of Advanced Science and Technology*, *77*, 7–24.

[20]. Garson, G. (1991). Interpreting neural-network connection weights. *AI Expert 6(4):46–51*, 1991.

[21]. Golewski, G. L. (2022). The Specificity of Shaping and Execution of Monolithic Pocket Foundations (PF) in Hall Buildings. *Buildings*, *12*(2).

[22]. Golewski, G. L. (2023a). Combined Effect of Coal Fly Ash (CFA) and Nanosilica (nS) on the Strength Parameters and Microstructural Properties of Eco-Friendly Concrete. *Energies*, *16*(1).

[23]. Golewski, G. L. (2023b). Concrete Composites Based on Quaternary Blended Cements with a Reduced Width of Initial Microcracks. *Applied Sciences (Switzerland)*, *13*(12).

[24]. Golewski, G. L. (2023c). Mechanical properties and brittleness of concrete made by combined fly ash, silica fume and nanosilica with ordinary Portland cement. *AIMS Materials Science*, *10*(3), 390–404.

[25]. Golewski, G. L. (2023d). The Phenomenon of Cracking in Cement Concretes and Reinforced Concrete Structures: The Mechanism of Cracks Formation, Causes of Their Initiation, Types and Places of Occurrence, and Methods of Detection—A Review. *Buildings*, *13*(3).

[26]. Gupta, R., & Trivedi, A. (2009). Bearing capacity and settlement of footing resting on confined loose silty sands. *Electronic Journal of Geotechnical Engineering*, *14 A*, 1–17.

[27]. Haeri, H., & Sarfarazi, V. (2016). The deformable multilaminate for predicting the Elasto-Plastic behavior of rocks. *Computers and Concrete*, *18*(2), 201–214.

[28]. Haeri, H., Shahriar, K., Marji, M. F., & Moarefvand, P. (2013). Simulating the bluntness of TBM Disc Cutters in Rocks using Displacement Discontinuity Method. *13th International Conference on Fracture 2013, ICF 2013*, *2*, 1414–1423.

[29]. Henzinger, C., & Heyer, D. (2018). Soil improvement using recycled aggregates from demolition waste. *Proceedings of the Institution of Civil Engineers: Ground Improvement*, *171*(2), 74–81.

[30]. https://firagiel.com/web/technical-software/agiel-neural-network/. (n.d.).

[31]. Iqbal, M. R., Hashimoto, K., Tachibana, S., & Kawamoto, K. (2019). Geotechnical properties of sludge blended with crushed concrete and incineration ash. *International Journal of GEOMATE*, *16*(57), 116–123.

[32]. Islam, A., Fahim Badhon, F., Abedin, Z., Islam, M.

A., Badhon, F. F., & Abedin, M. Z. (2017). Relation between Effective Particle Size and Angle of Internal Friction of Cohesionless Soil. *Architecture and Civil Engineering*, (April 2020). Retrieved from https://www.researchgate.net/publication/340903320

[33]. Jain, A., & Chawda, A. (2016). Apraisal of Demolished Concrete Coarse and Fines for Stabilization of Clayey Soil. *International Journal of Engineering Sciences & Research Technology*, *5*(9), 715–719.

[34]. Jain, R. K. (2013). A Study on Eco Friendly use of Recycled Rubber Tyres. *Direct Research Journal of Engineering and Information Technology*, *1*(2), 23–37.

[35]. Karkush, M. O., & Yassin, S. (2019). Improvement of Geotechnical Properties of Cohesive Soil Using Crushed Concrete. *Civil Engineering Journal*, *5*(10), 2110–2119.

[36]. Ladd, R. (1979). Preparing test specimens using undercompaction. *International Journal of Rock Mechanics and Mining Sciences & Geomechanics Abstracts*, *16*(3), 50.

[37]. Mullins, G., Winters, D., & Dapp, S. (2006). Predicting End Bearing Capacity of Post-Grouted Drilled Shaft in Cohesionless Soils. *Journal of Geotechnical and Geoenvironmental Engineering*, *132*(4), 478–487.

[38]. Olden, J. D., & Jackson, D. A. (2002). Illuminating the "black box": A randomization approach for understanding variable contributions in artificial neural networks. *Ecological Modelling*, *154*(1–2), 135–150. https://doi.org/10.1016/S0304-3800(02)00064-9

[39]. Ornek, M., Laman, M., Demir, A., & Yildiz, A. (2012). Prediction of bearing capacity of circular footings on soft clay stabilized with granular soil. *Soils and Foundations*, *52*(1), 69–80. https://doi.org/10.1016/j.sandf.2012.01.002

[40]. Sarfarazi, V., & Haeri, H. (2018). Three-dimensional numerical modeling of effect of bedding layer on the tensile failure behavior in hollow disc models using Particle Flow Code (PFC3D). *Structural Engineering and Mechanics*, *68*(5), 537–547.

[41]. Sarfarazi, V., Haeri, H., Ebneabbasi, P., Bagher Shemirani, A., & Hedayat, A. (2018). Determination of tensile strength of concrete using a novel apparatus. *Construction and Building Materials*, *166*, 817–832.

[42]. Sethy, B. P., Patra, C., Das, B. M., & Sobhan, K. (2021). Prediction of ultimate bearing capacity of circular foundation on sand layer of limited thickness using artificial neural network. *International Journal of Geotechnical Engineering*, *15*(10), 1252–1267.

[43]. Sharma, A., & Sharma, R. K. (2020). Strength and Drainage Characteristics of Poor Soils Stabilized with Construction Demolition Waste. *Geotechnical and Geological Engineering*, *38*(5), 4753–4760. https://doi.org/10.1007/s10706-020-01324-3

[44]. Sharma, V., Kumar, A., & Kapoor, K. (2019). Sustainable deployment of crushed concrete debris and geotextile to improve the load carrying capacity of granular soil. *Journal of Cleaner Production*, *228*, 124–134.

[45]. Soni, H., Saini, A., & Yadav, J. S. (2022). Behaviour of Square Footing Over Recycled Concrete Aggregate Resting on Loose Sand: Integrated Experimental and Numerical Analyses. *International Journal of Geosynthetics and Ground Engineering*, *8*(5), 1–16.

[46]. Swarna, S., Tezeswi, T. P., & Kumar, S. (2022). Implementing construction waste management in India: An extended theory of planned behaviour approach. *Environmental Technology and Innovation*, *27*(February), 102401.

[47]. Tabatabaie Shourijeh, P., Masoudi Rad, A., Heydari Bahman Bigloo, F., & Binesh, S. M. (2022). Application of recycled concrete aggregates for stabilization of clay reinforced with recycled tire polymer fibers and glass fibers. *Construction and Building Materials*, *355*(May), 129172.

[48]. Thakur, A., & Dutta, R. K. (2021). Study of bearing capacity of skirted irregular pentagonal footings on different sands. *Journal of Achievements in Materials and Manufacturing Engineering*, *1*(105), 5–17.

[49]. Verma, G., & Kumar, B. (2023). Artificial Neural Network Equations for Predicting the Modified Proctor Compaction Parameters of Fine-Grained Soil. *Transportation Infrastructure Geotechnology*, *10*, 424–447.

[50]. Wang, L., Zhang, P., Golewski, G., & Guan, J. (2023). Editorial: Fabrication and properties of concrete containing industrial waste. *Frontiers in Materials*, *10*(March), 2022–2023.

[51]. Yadav, J. S, Garg, A., & Tiwari, S. K. (2019). Strength and ductility behaviour of rubberised cemented clayey soil Authors. *Proceedings of the Institution of Civil Engineers - Ground Improvement*.

[52]. Yadav, Jitendra Singh. (2020). Feasibility study on utilisation of clay–waste tyre rubber mix as construction material. *Proceedings of the Institution of Civil Engineers - Construction Materials*, 1–13. https://doi.org/10.1680/jcoma.19.00114

[53]. Yadav, Jitendra Singh, & Tiwari, S. K. (2016). Behaviour of cement stabilized treated coir fibre-reinforced clay-pond ash mixtures. *Journal of Building Engineering*, *8*, 131–140.

[54]. Zhang, G., Ding, Z., Zhang, R., Chen, C., Fu, G., Luo, X., Wang, Y., & Zhang, C. (2022). Combined Utilization of Construction and Demolition Waste and Propylene Fiber in Cement-Stabilized Soil. *Buildings*, *12*(3). https://doi.org/10.3390/buildings12030350

ظرفیت باربری پایه دایره‌ای بر روی مواد زباله ساختمانی بازیافتی با استفاده از روش ANN

آنانت سایینی[۱] و جیتندرا سینگ یاداو[۲*]

۱. گروه مهندسی عمران، موسسه ملی فناوری حمیرپور، هیماچال پرادش، هند
۲. گروه مهندسی عمران، موسسه ملی فناوری کوروکشترا، هاریانا، هند

ارسال ۲۰۲۳/۰۸/۰۹، پذیرش ۲۰۲۳/۱۱/۰۷

* نویسنده مسئول مکاتبات: jsyadav@nitkkr.ac.in

چکیده:

هدف از این کار تحقیقاتی استفاده از یک مدل شبکه عصبی مصنوعی (ANN) برای پیش‌بینی ظرفیت باربری نهایی پایه دایره‌ای است که روی نخاله ساخت‌وساز بازیافتی روی شن و ماسه شل قرار دارد. مجموعه‌ای از آزمایش‌های بار صفحه با تغییر ضخامت دو اندازه از نخاله ساختمانی بازیافتی (۵ میلی‌متر و ۱۰.۶ میلی‌متر) لایه (d۰.۴، d۰.۶، d۰.۸، d۱، و d۱.۲، d: قطر پایه) انجام شد. در تراکم‌های نسبی مختلف (۳۰٪، ۵۰٪ و ۷۰٪) پوشش. ظرفیت باربری نهایی به دست آمده برای ترکیب‌های مختلف برای توسعه مدل ANN استفاده شد. پارامترهای ورودی مدل شبکه عصبی مصنوعی ضخامت لایه زباله ساختمانی بازیافتی به قطر نسبت پایه دایره‌ای، زاویه اصطکاک داخلی ماسه، وزن واحد شن، زاویه اصطکاک داخلی نخاله ساختمانی بازیافتی و وزن واحد نخاله ساختمانی بازیافتی، و پارامتر خروجی مدل ظرفیت باربری نهایی بود. با توجه به یافته‌های ANN، مدل FANN-SIGMOD_SYMMETRIC با توپولوژی ۳-۲-۱ تخمین بالاتری از ظرفیت باربری نهایی پایه دایره‌ای ارائه کرد. تجزیه و تحلیل حساسیت همچنین نشان داد که وزن واحد ماسه و زاویه اصطکاک داخلی ماسه تأثیر ناچیزی بر ظرفیت باربری نهایی دارد. ظرفیت باربری نهایی تخمین زده شده بیشتر تحت تأثیر زاویه اصطکاک داخلی زباله‌های ساخت و ساز بازیافتی قرار گرفت. نتیجه تحلیل رگرسیون خطی چندگانه به خوبی مدل ANN در پیش‌بینی ظرفیت باربری نهایی نبود.

کلمات کلیدی: مواد زائد ساختمانی، پایه دایره ای، ظرفیت باربری، ANN، MLR.